Materials Advances

ROYAL SOCIETY OF CHEMISTRY

PAPER

View Article Online
View Journal | View Issue

Cite this: *Mater. Adv.*, 2022, 3, 5893

Tetra-coordinated boron-appended zinc(II)-salen: a highly selective fluorescence-based sensor for Sm^{3+} ions *via* sensitization†

Prakash Nayak,[a] Anna Chandrasekar Murali,[a] Vadapalli Chandrasekhar *[bc] and Krishnan Venkatasubbaiah *[a]

Received 9th May 2022,
Accepted 5th June 2022

DOI: 10.1039/d2ma00516f

rsc.li/materials-advances

Selective detection of metal ions is very important from the environmental and biological points of view. In this regard, selective discrimination between lanthanide ions is very difficult and challenging owing to their similar atomic radii. Herein, we report a tetra-coordinated boron-based salen ligand that shows selective fluorescence enhancement with Zn^{2+} ions. More interestingly, isolated zinc complex **6a** was able to detect Sm^{3+} ions selectively. The luminescence color of complex **6a** changed from green to red upon addition of Sm^{3+} ions, which makes this design highly selective in discriminating Sm^{3+} ions in the presence of other lanthanide ions at a very low concentration of 1×10^{-5} M.

Introduction

In recent years, the design and synthesis of tri- and tetra-coordinated boron compounds have received considerable attention due to their applications in diverse fields such as light-emitting devices, photovoltaics, sensors and organic field-effect transistors.[1] The ability to attain a planar conformation, stability due to saturation of Lewis acidity and rigidity of the basic structure makes tetra-coordinated boron-based fluorophores more favorable alternatives over three-coordinated boron compounds. Among the different tetra-coordinated boron compounds, B–N coordinated compounds have secured considerable attention because of their widespread applications.[2] We and others have recently shown that B–N coordinated compounds can show oxygen sensing behavior, photochromism, non-linear optical properties *etc.*[2a,g,i,l,m,3]

Selective detection of metal ions has emerged as an important area of research due to its implications in the area of environmental, biological and clinical studies. Several probes or sensors have been reported for the detection of different metal ions employing colorimetric and/or fluorometric techniques.[4] Fluorescence-based probes or sensors have received considerable attention owing to their simplicity, selectivity and sensitivity towards specific metal ions. Among the different metal ions, lanthanide ions constitute a family with a very similar and a non-discriminative coordination behavior. On the other hand, the use of lanthanides in industrial applications is ever burgeoning, including in magnetism, displays, components of nuclear control rods and even as catalysts to name a few.[5] As some or many of the lanthanide ions are toxic in nature their detection is an important task. Although there are reports on the detection of different lanthanide ions,[6] selective discrimination and detection of lanthanide ions is a major challenge in view of their similarity in terms of size and chemical behavior.

Taking advantage of the emissive and electron-transporting properties of the B–N coordinated fluorophores with the chelating ability of salen ligands, which can find use in catalysis and materials chemistry, we designed a tetra-coordinated boron-functionalized pyrazole-based salen ligand (Fig. 1). We envisioned that this molecular architecture will enable the selective detection of Zn^{2+} using pocket 1 and also further expected that pocket 2 will discriminate lanthanide ions.

Results and discussion

Selective detection of zinc ion plays a vital role in the chemical and biological sciences owing to its important role in gene expression, apoptosis, cellular metabolism and neurotransmission.[7] A number of analytical techniques such as UV/Vis, fluorescence, atomic

[a] *School of Chemical Sciences, National Institute of Science Education and Research (NISER), an OCC of HOMI Bhabha National Institute, Bhubaneswar-752050, Odisha, India. E-mail: krishv@niser.ac.in*
[b] *Tata Institute of Fundamental Research Hyderabad, Gopanpally, Hyderabad-500 046, India*
[c] *Department of Chemistry, Indian Institute of Technology Kanpur, Kanpur-208016, India*

† Electronic supplementary information (ESI) available: Experimental procedures, spectroscopic data, and copies of the ^{1}H and ^{13}C NMR spectra. CCDC 2152949 and 2152950. For ESI and crystallographic data in CIF or other electronic format see DOI: https://doi.org/10.1039/d2ma00516f

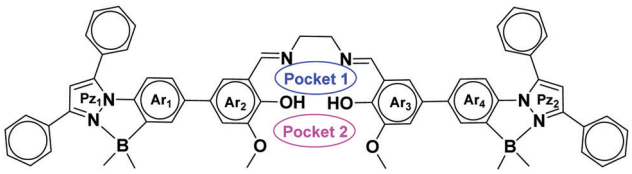

Fig. 1 Structure of the ligand used in this study.

absorption spectroscopy, and electrochemical methods are used for the detection of Zn^{2+} ions.[8] Among the different methods, fluorescent sensors have shown superior sensitivity. This motivated us to investigate the coordinating ability of boron functionalized compound **5a** as a luminescent probe for Zn^{2+}. The synthetic route to pyrazole-based boron functionalized imine ligand **5a** is outlined in Scheme 1. Compounds **1–3** were prepared according to the literature reported methods.[3g] Treatment of **2** and **3a** (Scheme S1, ESI†) with Na_2CO_3 and a catalytic amount of $Pd(PPh_3)_4$ under Suzuki coupling conditions resulted in a moderate yield (61%) of **4a**. Synthesis of the required ligand **5a** (Scheme 1) was achieved in an excellent yield (92%) by a simple condensation reaction of 2 equivalents of **4a** with ethylene diamine in dry methanol as a solvent. Compound **5a** was characterized using multi-nuclear NMR and HRMS. Furthermore, compound **5a** was also analysed using ^1H–^1H COSY (Fig. S8, ESI†).

The UV/Vis absorption and fluorescence spectra of **5a** (10 μM) reveal an absorption maximum at 330 nm and an emission maximum at 464 nm. To understand the sensing properties of **5a**, the absorption and fluorescence spectra of **5a** were recorded with different amounts of Zn^{2+} ions. Sequential addition of Zn^{2+} ions (0–2.4 eq.) to **5a** resulted in a new absorption peak at 353 nm with an isobestic point at 339 nm (Fig. S2, ESI†). As shown in Fig. 2, the fluorescence intensity gradually increased with sequential addition of Zn^{2+} ions (0–2.4 eq.). Furthermore, a selectivity test was performed using various cations such as Cd^{2+}, Co^{2+}, Fe^{3+}, Fe^{2+}, Hg^{2+}, K^+, Mn^{2+}, Cr^{3+}, Na^+, Ni^{2+} and Mg^{2+} to investigate the binding interaction of **5a** (10 μM). As shown in Fig. 2(c), only Zn^{2+} caused an enhanced emission, while other cations were silent. This result indicates that **5a** discriminates Zn^{2+} from other cations, which can be detected by green emission.

To determine the binding mode of the zinc ion with salen, we independently synthesized (Scheme 2) the Zn-salen and characterized it using different techniques like ^1H, ^{13}C, and ^{11}B. The disappearance of the OH peak at 13.61 ppm of ligand **5a** and the up-field shifting of four ethylene protons from 3.94 ppm in **5a** to 3.74 ppm in **6a** confirms the formation of

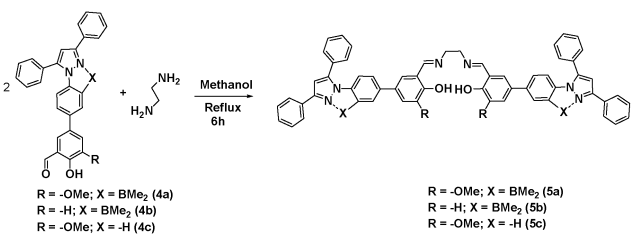

Scheme 1 Synthesis of ligands **5a–5c**.

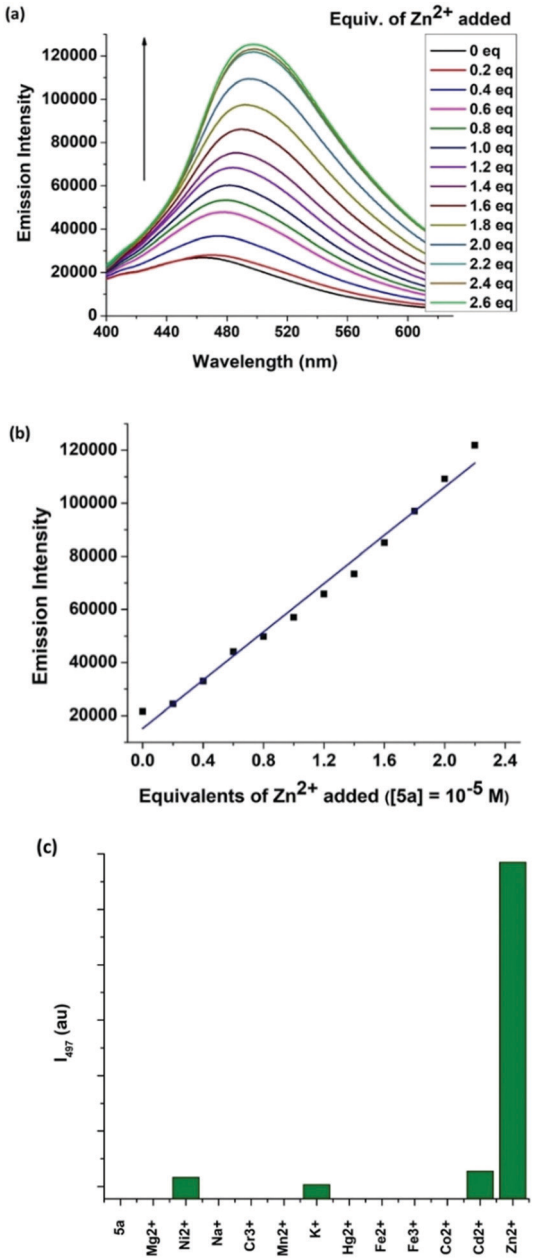

Fig. 2 (a) Fluorescence spectra (λ_{ex} = 330 nm) of **5a** (10 μM) with 2.2 equiv. of NaOAc upon addition of 0–2.4 equiv. of Zn^{2+} in the (10 : 90) methanol/THF solvent system. (b) Linear increase of the fluorescence intensity at 497 nm of **5a** (10 μM) upon addition of 0–2.4 equiv. of Zn^{2+} (λ_{ex} = 330 nm). (c) Fluorescence intensity profile changes of **5a** in the presence of 10 μM concentration of various metal ions at room temperature (λ_{ex} = 330 nm).

Zn^{2+} complex, **6a**. To our delight X-ray quality crystals of complex **6a** could be grown in the DMF/CH_3CN solvent system. The crystal structure confirms a 1 : 1 binding of **5a** with Zn^{2+} (Fig. S1, ESI†). The detection limit for Zn^{2+} was calculated and found to be 72 nM. These results reveal the applicability of **5a** in determining Zn^{2+} ions with high selectivity.

Complex **6a** crystallizes in a triclinic $P\bar{1}$ space group. The molecular structure reveals that the zinc atom adopts a

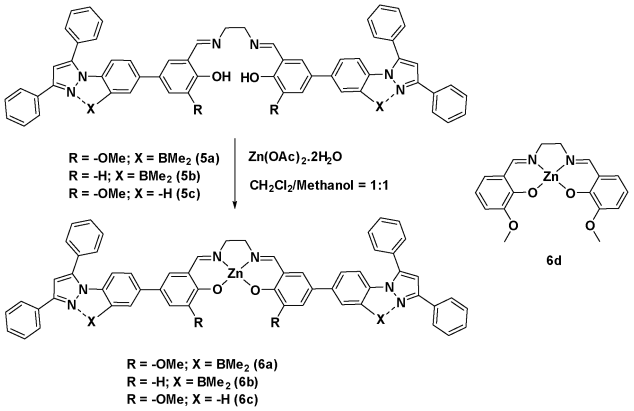

Scheme 2 Synthesis of zinc complexes **6a–6c** and structure of the complex **6d** used in this study.

five-coordinate distorted square pyramidal geometry. The zinc atom is 0.447 Å above the plane formed by N_2O_2 coordination from the salen motif. The axial position is occupied by a water molecule with the bond length of 2.066 Å. The Zn–O/N bond distances and angles observed for compound **6a** are consistent with previously reported Zn^{2+}-salen complexes.[9] The pyrazoles (Fig. 1, Pz_1 and Pz_2) and the *N*-phenyls (Fig. 1, Ar_1 and Ar_4) form a three cycle co-planarized system *via* B–N coordination. The torsional angles observed for Ar_3–Ar_4 and Ar_2–Ar_1 are 18.5° and 32.3°, respectively, which indicates that Zn-salen and the B–N coordinated pyrazole moieties have slight deviation from planarity.

With this success, we further investigated the coordination ability of pocket 2 in **6a** towards lanthanide ions. To our surprise complex **6a** discriminated lanthanide ions and was able to detect $\mathbf{Sm^{3+}}$ ions selectively using pocket 2. We examined the emission spectra of complex **6a** upon addition of 1.2 equiv. of various lanthanide ions such as $\mathbf{Sm^{3+}}$, Ce^{3+}, Dy^{3+}, Er^{3+}, Eu^{3+}, Gd^{3+}, Ho^{3+}, La^{3+}, Pr^{3+}, Tb^{3+}, Tm^{3+} and Yb^{3}. Except for $\mathbf{Sm^{3+}}$ ions, all other ions showed a weak fluorescence quenching at 500 nm (Fig. 3). However, a strong fluorescence quenching at 500 nm and enhanced emission peaks at 560 nm, 602 nm and 645 nm were observed on addition of 1.2 equivalents of $\mathbf{Sm^{3+}}$ ions to complex **6a**. This could be due to an efficient energy transfer from **6a** to the $\mathbf{Sm^{3+}}$ center upon complexation. These are characteristic peaks of $\mathbf{Sm^{3+}}$ emission resulting from the deactivation of the $^4G_{5/2}$ excited state to the ^6H_J ground state (J = 9/2, 7/2, and 5/2).[10] To determine the capability of **6a** to detect $\mathbf{Sm^{3+}}$ in an aqueous medium, 1.5 equivalents of $\mathbf{Sm^{3+}}$ ions in water were added to **6a** in THF solution, which showed an emission reminiscent of the methanol/THF system. This result suggests that **6a** can also be used to discriminate lanthanide ions in the THF/H_2O medium.

In general, the lanthanide ion sensitization process takes place from the triplet state of the sensitizer.[11] To understand the electronic properties of complex **6a**, and the sensitization phenomenon, TD-DFT calculations were performed using the optimized ground-state geometry of **6a**. The T1 triplet energy of complex **6a** was predicted using the corresponding TD-DFT

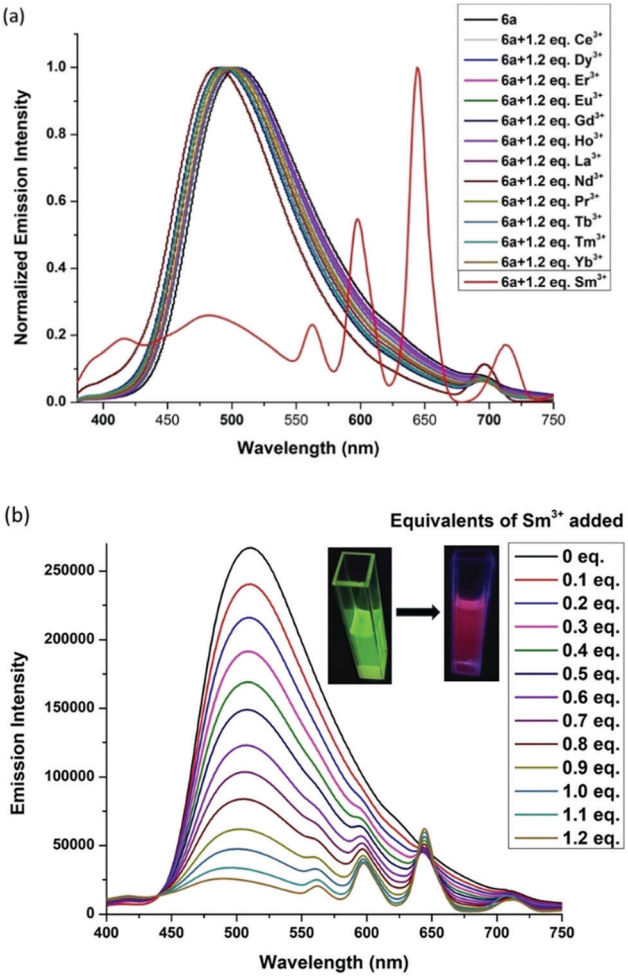

Fig. 3 (a) Normalized fluorescence spectra of **6a** (10 μM) upon the addition of different lanthanide ions (1.2 eq.) in (10 : 90) methanol/THF (λ_{ex} = 357). (b) Emission spectra of **6a** + $\mathbf{Sm^{3+}}$ in (10 : 90) methanol/THF with increasing concentrations of $\mathbf{Sm^{3+}}$ ions (**6a** concentration of 1×10^{-5} M); (insets) color changes under a UV lamp of **6a** and **6a** + 1.2 equiv. $\mathbf{Sm^{3+}}$ at 1×10^{-5} M concentration in (10 : 90) methanol/THF.

calculation results of **6a**, which gives an energy of 1053 nm/9497 cm^{-1} (Table S2, ESI†). The triplet state energy of **6a** is lower than the emissive state of $\mathbf{Sm^{3+}}$ ions (558 nm/17 900 cm^{-1}), which proves that the sensitization of $\mathbf{Sm^{3+}}$ by **6a** is not taking place from the triplet state. Previous reports have also shown that the sensitization of Ln^{3+} centers can occur from the singlet state of the sensitizers.[12] From TD-DFT calculations, it was calculated that the S1 singlet state energy of **6a** (388 nm/25 773 cm^{-1}) is above the emissive state $^4G_{5/2}$ of $\mathbf{Sm^{3+}}$. Thus, complex **6a** is expected to sensitize $\mathbf{Sm^{3+}}$ emission from its singlet S1 state.

In order to investigate the interactions between **6a** and $\mathbf{Sm^{3+}}$, we reacted complex **6a** with $Sm(NO_3)_3{\cdot}6H_2O$ in a 1 : 1.5 ratio in the $CHCl_3$/EtOH solvent system at room temperature and isolated pure **6a**·$\mathbf{Sm^{3+}}$ complex as a yellow precipitate. Single crystals of **6a**·$\mathbf{Sm^{3+}}$ were grown by slow evaporation of DMF and methanol. To our delight, single-crystal X-ray diffraction analysis revealed the formation of a 1 : 1 adduct, in which $\mathbf{Sm^{3+}}$ forms

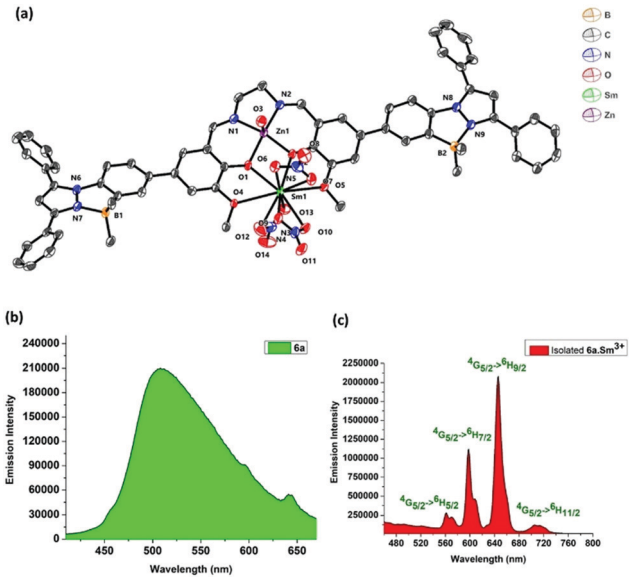

Fig. 4 (a) Crystal structure of the **6a·Sm^{3+}** complex. Thermal ellipsoids are drawn at the 50% probability level. Hydrogen atoms are removed for clarity. Solid-state emission spectra of complexes (b) **6a** and (c) **6a·Sm^{3+}**.

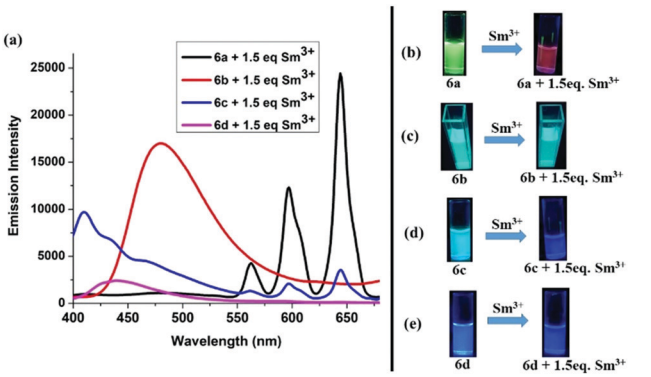

Fig. 5 (a) Fluorescence spectra of **6a–6d** with 1.5 equiv. of **Sm^{3+}** ions in (10 : 90) methanol/THF, concentration = 1×10^{-5} M. (b–e) Color changes under a UV lamp of **6a** and **6a** + 1.5 equiv. **Sm^{3+}**; **6b** and **6b** + 1.5 equiv. **Sm^{3+}**; **6c** and **6c** + 1.5 equiv. **Sm^{3+}**; **6d** and **6d** + 1.5 equiv. **Sm^{3+}** at 1×10^{-5} M ion concentration in (10 : 90) methanol/THF.

a nine-coordinated complex with **6a** (Fig. 4). Complex **6a·Sm^{3+}** crystallizes in the monoclinic system with a space group of $P2_1/c$. The complex **6a** is bound to the samarium ion through four oxygen atoms, in which the Sm1–O4 (2.667(4) Å) and Sm1–O5 (2.770(4) Å) bond distances are significantly longer than the Sm1–O1 (2.372(4) Å) and Sm1–O2 (2.357(3) Å) bond distances. The samarium ion is further coordinated to three nitrate ions adopting a distorted square pyramidal structure achieving a coordination number of nine. The zinc ion adopts a distorted square pyramidal coordination environment in the heterometallic complex. The Sm···Zn distance is 3.454 Å, suggesting that there is no direct Sm···Zn bond.

To determine the solid state emission properties of the **6a·Sm^{3+}** complex, we excited the complex at 350 nm. The solid state emission of **6a·Sm^{3+}** shows well-resolved peaks at 562 nm, 598 nm, 646 nm and 712 nm, which correspond to the transitions, $^4G_{5/2} \rightarrow {}^6H_{5/2}$, $^4G_{5/2} \rightarrow {}^6H_{7/2}$, $^4G_{5/2} \rightarrow {}^6H_{9/2}$ and $^4G_{5/2} \rightarrow {}^6H_{11/2}$, respectively. Among the emission peaks, the most intense emission at 645 nm corresponds to the $^4G_{5/2} \rightarrow {}^6H_{9/2}$ transition (Fig. 4). The complex **6a** showed green emission whereas **6a·Sm^{3+}** shows red emission in the solid state (Fig. 4).

The –OMe functionality plays an important role in forming the complex with **Sm^{3+}** ions. To test our hypothesis, we made compound **6b** (Scheme 2) which does not have any –OMe functionality. As expected, the emission of compound **6b** did not alter upon addition of **Sm^{3+}** ions (Fig. S5, ESI†). To investigate the importance of boron coordination, we synthesized complex **6c** (Scheme 2) that does not have boron in the framework and characterized it using ^{1}H and ^{13}C spectroscopy. Complex **6c** showed a blue-shifted absorption and emission with respect to **6a** (Fig. S7, ESI†). This signifies that boron coordination increases the rigidity of the pyrazole moiety, which resulted in slightly higher quantum yield and higher emission intensity for **6a** with respect to **6c** (Table S2, ESI†). When 1.5 equivalent of **Sm^{3+}** was added to **6c** (1×10^{-5} M), we observed very less intense **Sm^{3+}** characteristic peaks in the emission spectrum and some residual emission from **6c** (Fig. 5(a)). When the solution was kept under a hand held UV-lamp, no red emission was observed unlike for complex **6a** (Fig. 5(d)). When 1.5 equiv. of **Sm^{3+}** was added to **6a**, we observed intense **Sm^{3+}** characteristic peaks in the emission spectrum with no residual emission form **6a** and intense red emission under a hand held UV-lamp (Fig. 5(a and b)). We believe that non-radiative decay due to lack of rigidity in complex **6c** resulted in less intense red emission with respect to **6a**. The lack of rigidity in **6c** also resulted in inefficient energy transfer from the tri-phenyl pyrazole moiety to the **Sm^{3+}** center and thus caused relatively less intense red emission.

Dong and co-workers[6h] reported a bimetallic Zn–Sm complex derived from a Salamo-type ligand and also observed selective sensitization of the **Sm^{3+}** ions. Although structural characterization and emission for the Zn(II)–Sm(III) complex was presented, there is no discussion about the concentration of the solution used for this study. We synthesized compound **6d**, which is analogues to the complex of Dong and co-workers, and analysed its potential to test **Sm^{3+}** under identical conditions that we used in our study. Use of **6d** as a probe did not show any emission color change (conc. 1×10^{-5} M), when 1.5 equiv. of **Sm^{3+}** was added to the THF/methanol solution of **6d** (Fig. 5(a and e)). At the same time, **6a** made it possible to detect **Sm^{3+}** at 1×10^{-5} M concentration.

In order to compare the energy transfer in **6a**, **6c** and **6d**, we increased the concentration from 1×10^{-5} M to 5×10^{-5} M and plotted I_{644nm}/I_{Zn} (I_{zn} = emission maximum of the respective zinc complex) for all complexes with the addition of 1.5 equiv. **Sm^{3+}** ions. It was observed that the I_{644nm}/I_{Zn} ratio for **6a** + 1.5 equiv. **Sm^{3+}** is almost 100 times higher than that of **6d** and 20 times higher than that of **6c** at the same concentration. The inset emission spectra, shown in Fig. 6(a), reveal the presence of residual emission from **6c** at 484 nm and **6d** at 444 nm. This residual emission from **6c** and **6d** masks the red emission from

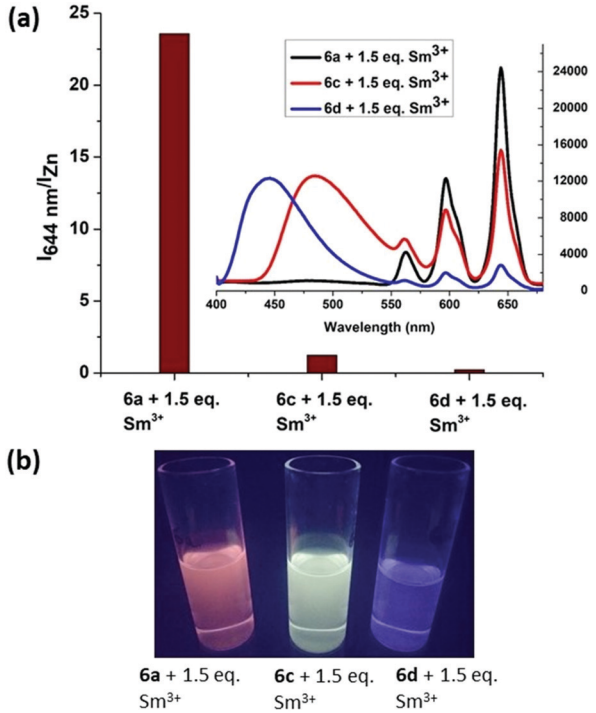

Fig. 6 (a) Comparing the energy transfer process in **6a**, **6c**, and **6d** with addition of 1.5 equiv. of Sm^{3+} at 5×10^{-5} M ion concentration in (10 : 90) methanol/THF. (b) Comparison of **6a**, **6c** and **6d** with 1.5 equiv. Sm^{3+} at 5×10^{-5} M concentration under a hand held UV-lamp.

Sm^{3+}, which can be observed under a hand held UV-Lamp (Fig. 6(b)). From these studies we conclude that our design has the advantage to discriminate Sm^{3+} ions at a very low concentration.

Conclusions

To conclude, we have successfully synthesized a tetra-coordinated boron-based salen ligand that exhibits excellent selectivity for the detection of Zn^{2+} ions using pocket 1. Furthermore, the zinc complex **6a**, showed remarkable luminescence response at a very low concentration upon the addition of Sm^{3+} ions and discriminates them from other lanthanide ions. X-Ray crystallography and other studies reveal that pocket 2 is responsible for the selective binding and sensitization of Sm^{3+} ions *via* a cooperative use of the B–N coordinated pyrazole motif and the –OMe functionality. The sensitivity of **6a** was found to be 100 fold that of **6d.** The design described here will be an excellent lead for the further development of ligands for the selective discrimination of metal ions.

Conflicts of interest

There are no conflicts to declare.

Acknowledgements

The authors thank the Department of Atomic Energy (DAE) for financial support. We thank Dr U. Louderaj for helpful discussion about DFT studies. We also thank Principal Scientist Dr R. Natarajan from IICB-Kolkata for his help with X-ray studies and Dr Mriganka Sadhukan for elemental analysis.

Notes and references

1 (*a*) F. Jäkle, *Chem. Rev.*, 2010, **110**, 3965–4022; (*b*) Y.-L. Rao, H. Amarne and S. Wang, *Coord. Chem. Rev.*, 2012, **256**, 759–770; (*c*) D. Li, H. Zhang and Y. Wang, *Chem. Soc. Rev.*, 2013, **42**, 8416–8433; (*d*) Z. M. Hudson and S. Wang, *Acc. Chem. Res.*, 2009, **42**, 1584–1596; (*e*) D. Frath, J. Massue, G. Ulrich and R. Ziessel, *Angew. Chem., Int. Ed.*, 2014, **53**, 2290–2310; (*f*) K. Tanaka and Y. Chujo, *NPG Asia Mater.*, 2015, **7**, e223; (*g*) P.-Z. Chen, L.-Y. Niu, Y.-Z. Chen and Q.-Z. Yang, *Coord. Chem. Rev.*, 2017, **350**, 196–216; (*h*) L. Ji, S. Griesbeck and T. B. Marder, *Chem. Sci.*, 2017, **8**, 846–863; (*i*) E. von Grotthuss, A. John, T. Kaese and M. Wagner, *Asian. J. Org. Chem.*, 2018, **7**, 37–53; (*j*) T. W. Hudnall, C.-W. Chiu and F. P. Gabbaï, *Acc. Chem. Res.*, 2009, **42**, 388–397; (*k*) J. F. Araneda, W. E. Piers, B. Heyne, M. Parvez and R. McDonald, *Angew. Chem., Int. Ed.*, 2011, **50**, 12214–12217; (*l*) X. Su, T. A. Bartholome, J. R. Tidwell, A. Pujol, S. Yruegas, J. J. Martinez and C. D. Martin, *Chem. Rev.*, 2021, **121**, 4147–4192; (*m*) R. R. Maar, R. Zhang, D. G. Stephens, Z. Ding and J. B. Gilroy, *Angew. Chem., Int. Ed.*, 2019, **58**, 1052–1056; (*n*) R. Zhao, C. Dou, Z. Xie, J. Liu and L. Wang, *Angew. Chem., Int. Ed.*, 2016, **55**, 5313–5317; (*o*) S. Sa, A. C. Murali, P. Nayak and K. Venkatasubbaiah, *Chem. Commun.*, 2021, **57**, 10170–10173.

2 (*a*) A. Wakamiya, T. Taniguchi and S. Yamaguchi, *Angew. Chem., Int. Ed.*, 2006, **45**, 3170–3173; (*b*) D. L. Crossley, I. A. Cade, E. R. Clark, A. Escande, M. J. Humphries, S. M. King, I. Vitorica-Yrezabal, M. J. Ingleson and M. L. Turner, *Chem. Sci.*, 2015, **6**, 5144–5151; (*c*) M. Grandl, T. Kaese, A. Krautsieder, Y. Sun and F. Pammer, *Chem. – Eur. J.*, 2016, **22**, 14373–14382; (*d*) S. K. Mellerup, K. Yuan, C. Nguyen, Z. H. Lu and S. Wang, *Chem. – Eur. J.*, 2016, **22**, 12464–12472; (*e*) M. Yusuf, K. Liu, F. Guo, R. A. Lalancette and F. Jäkle, *Dalton. Trans.*, 2016, **45**, 4580–4587; (*f*) D. L. Crossley, R. Goh, J. Cid, I. Vitorica-Yrezabal, M. L. Turner and M. J. Ingleson, *Organometallics*, 2017, **36**, 2597–2604; (*g*) K. Liu, R. A. Lalancette and F. Jäkle, *J. Am. Chem. Soc.*, 2017, **139**, 18170–18173; (*h*) S. Schraff, Y. Sun and F. Pammer, *J. Mater. Chem. C*, 2017, **5**, 1730–1741; (*i*) J. Wang, B. Jin, N. Wang, T. Peng, X. Li, Y. Luo and S. Wang, *Macromolecules*, 2017, **50**, 4629–4638; (*j*) M. Mamada, G. Tian, H. Nakanotani, J. Su and C. Adachi, *Angew. Chem., Int. Ed.*, 2018, **57**, 12380–12384; (*k*) S. Wang, K. Yuan, M. F. Hu, X. Wang, T. Peng, N. Wang and Q. S. Li, *Angew. Chem., Int. Ed.*, 2018, **57**, 1073–1077; (*l*) B. P. Dash, I. Hamilton, D. J. Tate, D. L. Crossley, J.-S. Kim, M. J. Ingleson and M. L. Turner, *J. Mater. Chem. C*, 2019, **7**, 718–724; (*m*) Y. Li, H. Meng, T. Liu, Y. Xiao, Z. Tang, B. Pang, Y. Li, Y. Xiang, G. Zhang, X. Lu, G. Yu,

H. Yan, C. Zhan, J. Huang and J. Yao, *Adv. Mater.*, 2019, **31**, e1904585; (*n*) K. Liu, R. A. Lalancette and F. Jäkle, *J. Am. Chem. Soc.*, 2019, **141**, 7453–7462; (*o*) J. Full, S. P. Panchal, J. Gotz, A. M. Krause and A. Nowak-Krol, *Angew. Chem., Int. Ed.*, 2021, **60**, 4350–4357; (*p*) A. C. Murali, P. Nayak and K. Venkatasubbaiah, *Dalton. Trans.*, 2022, **51**, 5751–5771; (*q*) Z. Dominguez, R. Lopez-Rodriguez, E. Alvarez, S. Abbate, G. Longhi, U. Pischel and A. Ros, *Chem. – Eur. J.*, 2018, **24**, 12660–12668.

3 (*a*) C. Li, S. K. Mellerup, X. Wang and S. Wang, *Organometallics*, 2018, **37**, 3360–3367; (*b*) S. K. Mellerup, C. Li, X. Wang and S. Wang, *J. Org. Chem.*, 2018, **83**, 11970–11977; (*c*) X. Li, Y. Shi, N. Wang, T. Peng and S. Wang, *Chem. – Eur. J.*, 2019, **25**, 5757–5767; (*d*) Z. He, L. Liu, Z. Zhao, S. K. Mellerup, Y. Ge, X. Wang, N. Wang and S. Wang, *Chem. – Eur. J.*, 2020, **26**, 12403–12410; (*e*) M. Vanga, S. Sa, A. Kumari, A. C. Murali, P. Nayak, R. Das and K. Venkatasubbaiah, *Dalton Trans.*, 2020, **49**, 7737–7746; (*f*) D. Kunchala, S. Sa, P. Nayak, J. Ponniah and S. K. Venkatasubbaiah, *Organometallics*, 2019, **38**, 870–878; (*g*) V. Mukundam, S. Sa, A. Kumari, R. Das and K. Venkatasubbaiah, *J. Mater. Chem. C*, 2019, **7**, 12725–12737.

4 (*a*) K. P. Carter, A. M. Young and A. E. Palmer, *Chem. Rev.*, 2014, **114**, 4564–4601; (*b*) L. Wang, X. Gong, Q. Bing and G. Wang, *Microchem. J.*, 2018, **142**, 279–287; (*c*) P. Ravichandiran, A. Boguszewska-Czubara, M. Masłyk, A. P. Bella, S. A. Subramaniyan, P. M. Johnson, K. S. Shim, H. G. Kim and D. J. Yoo, *ACS Sustainable Chem. Eng.*, 2019, **7**, 17210–17219; (*d*) N. Yadav and A. K. Singh, *J. Electrochem. Soc.*, 2019, **166**, B644–B653; (*e*) A. Gul, M. Oguz, A. N. Kursunlu and M. Yilmaz, *Dyes Pigm.*, 2020, **176**, 108221; (*f*) M. Sahu, A. Kumar Manna, K. Rout, J. Mondal and G. K. Patra, *Inorg. Chim. Acta*, 2020, **508**, 119633; (*g*) Y. Zhang, W. Wang, R. Li, E. Zhang, Z. Li, L. Tang, B. Han, X. Hou and J. J. Wang, *Spectrochim. Acta, Part A*, 2020, **230**, 118050; (*h*) T. Samanta and R. Shunmugam, *Mater. Adv.*, 2021, **2**, 64–95.

5 (*a*) F. T. Edelmann, *Chem. Soc. Rev.*, 2012, **41**, 7649–7964; (*b*) J. Kido and Y. Okamoto, *Chem. Rev.*, 2002, **102**, 2357–2368; (*c*) S. Faulkner, S. J. A. Pope and B. P. Burton-Pye, *Appl. Spectrosc. Rev.*, 2005, **40**, 1–31; (*d*) C. Andraud and O. Maury, *Eur. J. Inorg. Chem.*, 2009, 4357–4371; (*e*) C. J. Weiss and T. J. Marks, *Dalton Trans.*, 2010, **39**, 6576–6588; (*f*) S. D. Bennett, B. A. Core, M. P. Blake, S. J. Pope, P. Mountford and B. D. Ward, *Dalton Trans.*, 2014, **43**, 5871–5885; (*g*) Z. Ahmed and K. Iftikhar, *Inorg. Chem.*, 2015, **54**, 11209–11225; (*h*) V. V. Utochnikova, N. N. Solodukhin, A. N. Aslandukov, L. Marciniak, I. S. Bushmarinov, A. A. Vashchenko and N. P. Kuzmina, *Org. Electron.*, 2017, **44**, 85–93; (*i*) F. Zinna, M. Pasini, F. Galeotti, C. Botta, L. Di Bari and U. Giovanella, *Adv. Funct. Mater.*, 2017, **27**, 1603719; (*j*) Y. Qiao and E. J. Schelter, *Acc. Chem. Res.*, 2018, **51**, 2926–2936; (*k*) Y. Zhang, S. Liu, Z.-S. Zhao, Z. Wang, R. Zhang, L. Liu and Z.-B. Han, *Inorg. Chem. Front.*, 2021, **8**, 590–619; (*l*) P. Kalita, J. Goura, J. M. Herrera, E. Colacio and V. Chandrasekhar, *ACS Omega*, 2018, **3**, 5202–5211; (*m*) A. K. Bar, P. Kalita, M. K. Singh, G. Rajaraman and V. Chandraselkar, *Coord. Chem. Rev.*, 2018, **367**, 163–216; (*n*) P. Kalita, N. Ahmed, A. K. Bar, S. Dey, A. Jana, G. Rajaraman, J.-P. Sutter and V. Chandrasekhar, *Inorg. Chem.*, 2020, **59**, 6603–6612; (*o*) V. V. Utochnikova, E. V. Latipov, A. I. Dalinger, Y. V. Nelyubina, A. A. Vashchenko, M. Hoffmann, A. S. Kalyakina, S. Z. Vatsadze, U. Schepers, S. Bräse and N. P. Kuzmina, *J. Lumin.*, 2018, **202**, 38–46; (*p*) L. Wang, Z. Zhao, C. Wei, H. Wei, Z. Liu, Z. Bian and C. Huang, *Adv. Opt. Mater.*, 2019, **7**, 1801256.

6 (*a*) D. A. Chowdhury, T. Ogata and S. Kamata, *Anal. Chem.*, 1996, **68**, 366–370; (*b*) C. E. Lisowski and J. E. Hutchison, *Anal. Chem.*, 2009, **81**, 10246–10253; (*c*) C. Han, L. Zhang and H. Li, *Chem. Commun.*, 2009, 3545–3547; (*d*) P. Das, A. Ghosh and A. Das, *Inorg. Chem.*, 2010, **49**, 6909–6916; (*e*) T. Gorai and U. Maitra, *Angew. Chem., Int. Ed.*, 2017, **56**, 10730–10734; (*f*) P. Harvey, A. Nonat, C. Platas-Iglesias, L. S. Natrajan and L. J. Charbonniere, *Angew. Chem., Int. Ed.*, 2018, **57**, 9921–9924; (*g*) G. I. Vargas-Zuniga and J. L. Sessler, Sensors for Lanthanides and Actinides, in *The Rare Earth Elements: Fundamentals and Applications*, ed. Atwood, D. A., Wiley, 2012, pp. 561–573; (*h*) S.-S. Zheng, W.-K. Dong, Y. Zhang, L. Chen and Y.-J. Ding, *New J. Chem.*, 2017, **41**, 4966–4973.

7 (*a*) M. P. Cuajungco and G. J. Lees, *Neurobiol. Dis.*, 1997, **4**, 137–169; (*b*) D. Beyersmann and H. Haase, *Biometals*, 2001, **14**, 331–341; (*c*) D. Beyersmann, *Materialwiss. Werkstofftech.*, 2002, **33**, 764–769; (*d*) S. G. Bell and B. L. Vallee, *ChemBioChem*, 2009, **10**, 55–62; (*e*) W. Maret, *Biometals*, 2011, **24**, 411–418; (*f*) W. Maret, *Adv. Nutr.*, 2013, **4**, 82–91; (*g*) S. Triboulet, C. Aude-Garcia, L. Armand, A. Gerdil, H. Diemer, F. Proamer, V. Collin-Faure, A. Habert, J. M. Strub, D. Hanau, N. Herlin, M. Carriere, A. Van Dorsselaer and T. Rabilloud, *Nanoscale*, 2014, **6**, 6102–6114; (*h*) T. Kambe, T. Tsuji, A. Hashimoto and N. Itsumura, *Physiol. Rev.*, 2015, **95**, 749–784; (*i*) W. Maret, *Metallomics*, 2015, **7**, 202–211; (*j*) L. C. Costello and R. B. Franklin, *Arch. Biochem. Biophys.*, 2016, **611**, 100–112; (*k*) K. Grüngreiff, D. Reinhold and H. Wedemeyer, *Ann. Hepatol.*, 2016, **15**, 7–16; (*l*) W. Maret, *Int. J. Mol. Sci.*, 2017, **18**, 2285; (*m*) X. Yang, H. Wang, C. Huang, X. He, W. Xu, Y. Luo and K. Huang, *Sci. Rep.*, 2017, **7**, 14669; (*n*) W. Maret, *Free Radical Biol. Med.*, 2019, **134**, 311–326.

8 (*a*) K. Hanaoka, K. Kikuchi, H. Kojima, Y. Urano and T. Nagano, *Angew. Chem., Int. Ed.*, 2003, **42**, 2996–2999; (*b*) Y. Xu, J. Meng, L. Meng, Y. Dong, Y. Cheng and C. Zhu, *Chem. – Eur. J.*, 2010, **16**, 12898–12903; (*c*) Z. Xu, K.-H. Baek, H. N. Kim, J. Cui, X. Qian, D. R. Spring, I. Shin and J. Yoon, *J. Am. Chem. Soc.*, 2010, **132**, 601–610.

9 (*a*) M. E. Germain, T. R. Vargo, P. G. Khalifah and M. J. Knapp, *Inorg. Chem.*, 2007, **46**, 4422–4429; (*b*) X.-Q. Song, Y.-Q. Peng, G.-Q. Cheng, X.-R. Wang, P.-P. Liu and W.-Y. Xu, *Inorg. Chim. Acta*, 2015, **427**, 13–21.

10 Y. Hasegawa, Y. Kitagawa and T. Nakanishi, *NPG Asia Mater.*, 2018, **10**, 52–70.

11 (*a*) E. A. Varaksina, I. V. Taydakov, S. A. Ambrozevich, A. S. Selyukov, K. A. Lyssenko, L. T. Jesus and R. O. Freire, *J. Lumin.*, 2018, **196**, 161–168; (*b*) Z. Ahmed and K. Iftikhar, *Dalton Trans.*, 2019, **48**, 4973–4986; (*c*) F. P. Aguiar, I. F. Costa, J. G. P. Espínola, W. M. Faustino, J. L. Moura, H. F. Brito, T. B. Paolini, M. C. F. C. Felinto and E. E. S. Teotonio, *J. Lumin.*, 2016, **170**, 538–546; (*d*) Z. Li, P. Li, Q. Xu and H. Li, *Chem. Commun.*, 2015, **51**, 10644–10647; (*e*) J.-C. G. Bünzli, *Coord. Chem. Rev.*, 2015, **293–294**, 19–47; (*f*) L. Sun, Y. Qiu, T. Liu, J. Feng, W. Deng and L. Shi, *Luminescence*, 2015, **30**, 1071–1076; (*g*) P. Kalita, P. Nayak, N. Ahmed, J. M. Herrera, K. Venkatasubbaiah, E. Colacio and V. Chandrasekhar, *Dalton Trans.*, 2020, **49**, 15404–15416.

12 (*a*) A. Guenet, F. Eckes, V. Bulach, C. A. Strassert, L. De Cola and M. W. Hosseini, *ChemPhysChem*, 2012, **13**, 3163–3171; (*b*) E. Kasprzycka, V. A. Trush, V. M. Amirkhanov, L. Jerzykiewicz, O. L. Malta, J. Legendziewicz and P. Gawryszewska, *Chem. – Eur. J.*, 2017, **23**, 1318–1330; (*c*) J. R. G. Thorne, J. M. Rey, R. G. Denning, S. E. Watkins, M. Etchells, M. Green and V. Christon, *J. Phys. Chem. A*, 2002, **106**, 4014–4021.